

# A Computational Study of Bubble Formation from an Orifice Submerged in Liquid with Constant Gas Flow

James Q. Feng

OXCBO Research, Maple Grove, Minnesota, USA

[james.q.feng@gmail.com](mailto:james.q.feng@gmail.com)

## Abstract

The process of bubble formation from an orifice submerged in liquid with constant gas flow is studied by numerical simulations using an OpenFOAM® volume-of-fluid solver named interIsoFoam. The computed results show that the detached bubble size tends to increase with the gas flow rate, orifice size, surface tension, liquid contact angle, etc. in qualitative agreement with most previous authors. For a given orifice size and liquid properties, there exists a critical gas flow rate above which detached bubbles will combine via coalescence known as bubble pairing. The detached bubble size seems insensitive to the contact angle when the liquid adequately wets the orifice wall, but can increase substantially if the contact angle is increased beyond a critical value resulting in contact line motion on the horizontal orifice surface. The value of such a critical contact angle increases with the orifice size as well as gas flow rate. Such revelations would logically suggest that the usage of reduced orifice size for generating smaller bubbles could be more challenging and practically difficult with constant gas flow for sub-millimeter orifices.

**Keywords:** bubble formation, submerged orifice, constant gas flow, volume-of-fluid

## 1 Introduction

Flowing a gas through an upward-facing orifice into a liquid tank usually generates a sequence of bubbles, which has become essential in a wide range of phase contacting applications as seen in bubble columns, sparger reactors, extraction equipment, water treatment, etc. In view of physics, a gas bubble grows with continuously flowing gas while attached along the contact line to the orifice wall before detaching, and freely rises in the liquid after the buoyancy force overcomes the capillary force. The size of detached bubble, however, can be influenced by many factors besides the balance of buoyancy and surface tension such as gas flow rate, orifice size, wetting property of liquid on the orifice wall, and so on. The bubble formation process involves complicated fluid dynamics with free surface deformation, disintegration, coalescence, as well as dynamic contact line motion. Its practical importance as well as theoretical modeling challenge has inspired numerous publications by generations of authors (cf. Harkins and Brown 1919; Clift et al. 1978; Gaddis and Vogelpohl 1986; Oguz and Prosperetti

1993; Ponter and Surati 1997; Kulkarni and Joshi 2005; Buwa et al. 2007; Ohta et al. 2011; Simmons et al. 2015). Along with ample experimental results, most theoretical models developed before 1980 were simplified based on force balances with spherically symmetric growing bubbles often assuming a quasi-static process for very low gas flow rate (as commented by Oguz and Prosperetti 1993; Buwa et al. 2007). To date, even with the available modern experimental equipment and numerical techniques, the general applicability of individually derived theoretical formulas remain elusive (Bari and Robinson, 2013). Due to the complexity of the dynamic process involved in bubble formation, improved understanding of the fundamental physics may only be achieved with more model investigations as well as redundant comparisons and cross-examinations.

To simulate the mathematically difficult free-boundary fluid dynamics with minimal simplifying assumptions, various numerical methods have been developed with the advent of high-speed computers. For bubbles forming in inviscid or highly viscous liquids governed by linear field equations, a boundary-element (or boundary-integral) method (BEM) in terms of Green's functions by discretizing only along the boundaries has been quite effective with results in apparent agreement with experiments (e.g., Oguz and Prosperetti 1993; Wong et al. 1998; Higuera 2005). The restriction to linear field equations can be eliminated by solving the full nonlinear Navier-Stokes equations with tessellation of entire problem domain, which led to the development of several versions of arbitrary Lagrangian-Eulerian (ALE) methods capable of dealing with large deformations of boundary shapes governed by nonlinear field equations (e.g., Kistler and Scriven 1983; Christodoulou and Scriven 1992) as exemplified in computing highly deformed bubbles (Feng 2007) and bubble formation dynamics (Simmons et al. 2015). However, the difficulties to compute the situation with free surface disintegration and coalescence with the ALE methods have motivated usage of the purely Eulerian methods such as volume of fluid (VOF by Hirt and Nichols 1981), level set method (LSM by Sussman et al. 1998), coupled level set and volume of fluid (CLSVOF by Sussman and Puckett 2000), for investigations of bubble dynamics (e.g. Krishna et al. 1999; Buwa et al. 2007; Nichita et al. 2010; Ohta et al. 2011; Sudeepta Vaishnavi et al. 2023). Unlike ALE with boundary-fitting moving meshes able to track free surface accurately, the resolution of free surface position in VOF simulations depends directly on the Eulerian mesh size; therefore, accurate free surface shape with VOF computation can usually be determined at the expense of a much finer mesh than typical ALE meshes.

Although effective numerical methodologies appear to be well established, most computational codes used in publications are not easily accessible. Code development from scratch even with well established methodologies can be very resource demanding, and almost prohibitive to most small organization researchers. Fortunately, several open source software packages have been available in recent years with computational capabilities comparable, or even superior, to commercial packages. Among others, the OpenFOAM<sup>®</sup> package consists of a variety of common solvers and boundary conditions, with powerful meshing utilities and postprocessing capabilities; it allows user to freely download the C++ source code for custom modifications to suit particular needs, with a large user base across engineering and scientific communities for exchanging knowledge. Hence, a recent version (v2206) of OpenFOAM<sup>®</sup> VOF solver is selected for self-consistent simulations of the bubble formation process in this work.

## 2 Computational Model Description

Considered here is a gas with a constant flow rate through an inlet tube connected to an orifice into a liquid tank, as shown in figure 1a. The two-phase fluid flow is assumed axisymmetric, enabling the use of a wedge type mesh (figure 1b) generated with the OpenFOAM<sup>®</sup> meshing utilities such as blockMesh, mergeMeshes and stitchMesh for combining fine and coarse mesh patches to reduce computational burden while the free surface location can be adequately resolved. The chosen solver for this type of two-phase flow problem is named interIsoFoam—an improved VOF solver detailed by Roenby et al. (2016), Gamet et al. (2020), and reviewed by Mulbah et al. (2022) as a scheme for high accuracy at low computational cost. Because the description of this type of VOF solver is available in published literature, it is unnecessary to repeat here beyond specifying the particular case parameters.

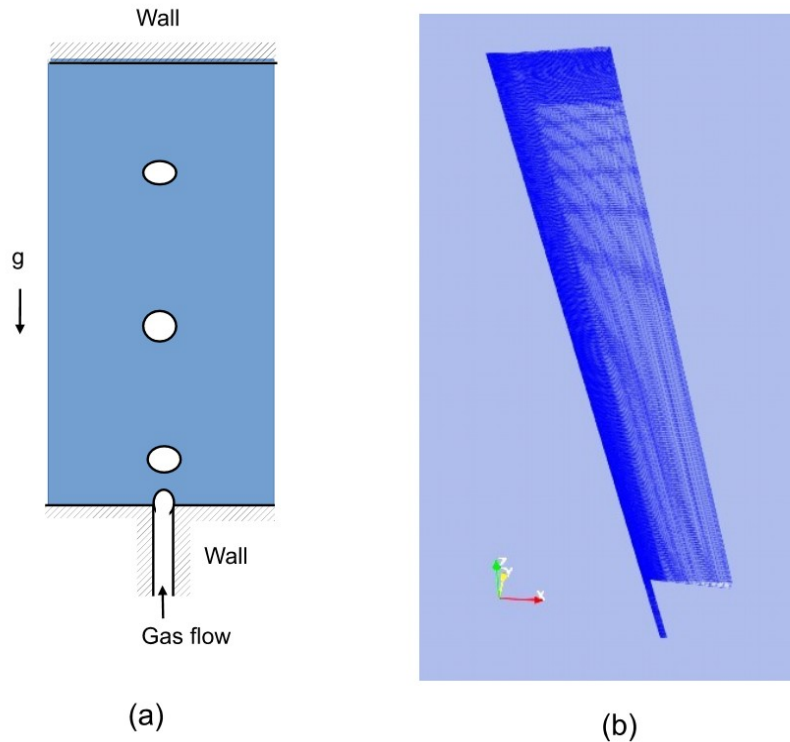


Figure 1. (a) Schematic of bubble formation when a gas flowing through an orifice into a liquid tank; (b) A wedge mesh combining fine and coarse mesh patches generated with the OpenFOAM<sup>®</sup> meshing utilities blockMesh, mergeMeshes and stitchMesh, used for simulations of the axisymmetric two-phase flows in the present bubble formation problem

In the present model, the nominal values for liquid phase density and dynamic viscosity are  $\rho = 1000 \text{ kg m}^{-3}$  and  $\mu = 0.001 \text{ kg m}^{-1} \text{ s}^{-1}$  (i.e., 1 cp), whereas those corresponding to the gas

phase are  $1.2 \text{ kg m}^{-3}$  and  $1.8 \times 10^{-5} \text{ kg m}^{-1} \text{ s}^{-1}$  (0.018 cp), respectively specified for the VOF computations. Over orders-of-magnitude contrasts between liquid and gas phases in terms of these corresponding values usually make gas-phase influence to the general fluid dynamical behavior almost irrelevant; therefore, only liquid density and viscosity are considered in the analysis and discussion. The value of surface tension at gas-liquid interface is taken as  $\sigma = 0.07 \text{ kg s}^{-2}$ , closely representing the air-water situation, unless otherwise specified.

To complete the case specification, the boundary conditions at gas inlet are uniform fixed value for velocity  $U_z = \text{constant}$  and zeroGradient for the piezometric pressure  $p$  (cf. Description in Feng 2017), at solid wall noslip for  $U$  and zeroGradient for  $p$ , at open lateral boundary a pressureInletOutletVelocity condition for  $U$  and a fixed value for  $p$  (e.g.,  $= 10^5 \text{ Pa}$ ). At the gas-liquid-solid three phase contact line, the dynamicAlphaContactAngle condition is applied by specifying the static contact angle  $\theta_0$ , advancing contact angle  $\theta_A$  and receding contact angle  $\theta_R$  as well as a  $u_\theta$  value. Here, for a specified static contact angle  $\theta_0$  the advancing contact angle and receding contact angle are always assigned as  $\theta_A = \theta_0 + 15^\circ$  and  $\theta_R = \theta_0 - 15^\circ$  with a fixed value of  $u_\theta$  (i.e.,  $= 1 \text{ m s}^{-1}$ ) to keep the presentation logically streamlined. Without losing generality, computed cases in the present work would have a nominal contact angle  $\theta_0 = 45^\circ$  (as a partially wetting liquid at the solid wall) unless otherwise specified.

Per OpenFOAM<sup>®</sup> solver development requirements, each solver must come with at least one tutorial case. In fact, many popular solvers could have multiple tutorial cases provided with the standard downloadable packages. This can be very convenient for users who would not want to spend much time in deciphering the exact meanings of numerical scheme parameters; some of those tutorial parameter settings can indeed be directly used for similar computational problems without need for modifications. For example, the numerical scheme parameters used in the present work for fvScheme and fvSolution are directly copied from the interIsoFoam tutorial case of “damBreak”.

### 3 Results and Discussion

Before computing numerical solutions, it is useful to estimate a few reference parameters often used in the literature (e.g., Oguz and Prosperetti 1993; Ohta et al. 2011; Simmons et al. 2015). According to a force balance between surface tension and buoyancy (Fritz 1935; van Krevelen and Hoftijzer 1950; Kumar and Kuloor 1970), the Fritz bubble volume  $V_F$  and corresponding bubble diameter  $d_F$  may be estimated with simple equations,

$$\sigma \pi d_c = \rho g V_F = \frac{\rho g \pi d_c^3}{6}, \text{ thus } V_F = \frac{\sigma \pi d_c}{\rho g} \text{ and } d_F = \left( \frac{6 \sigma d_c}{\rho g} \right)^{1/3}, \quad (1)$$

where  $\rho$  denotes the mass density of liquid,  $\sigma$  surface tension of the gas-liquid interface,  $g$  the acceleration of gravity, and  $d_c$  the diameter of three-phase contact line at orifice (which is often assumed to be the same as the orifice diameter  $D$ .)

The analysis of Oguz and Prosperetti (1993) suggested that the Fritz volume and diameter are expected to be only reasonable the quasi-static situation when the gas flow rate  $Q \ll Q_{crit}$  where the critical gas flow rate may be expressed as

$$Q_{crit} = \pi \left( \frac{16}{3g^2} \right)^{1/6} \left( \frac{\sigma D}{2\rho} \right)^{5/6} . \quad (2)$$

At high gas flow rates, i.e.,  $Q > Q_{crit}$ , the bubbles would detach with a volume proportional to  $Q^{6/5}$ .

In what follows, the nominal air-water system is examined first, with cases of variations in liquid viscosity, surface tension in the subsequent subsections.

### 3.1 Air bubbles in water

For air bubbles in water with  $\rho = 1000 \text{ kg m}^{-3}$ ,  $\sigma = 0.07 \text{ kg s}^{-2}$ ,  $g = 9.81 \text{ m s}^{-2}$ , and  $\mu = 0.001 \text{ kg m}^{-1} \text{ s}^{-1}$  the value of the Ohnesorge number,

$$Oh = \frac{\mu g^{1/4}}{\rho^{1/4} \sigma^{3/4}} , \quad (3)$$

becomes  $2.313 \times 10^{-3}$ , suggesting that the liquid viscosity effect in an air-water system is negligible and an inviscid fluid model for bubble formation can yield reasonable results in agreement with experiments (as shown by Oguz and Prosperetti 1993).

An interesting special situation is that of  $d_F = d_c$  which yields

$$d_F = d_c = \sqrt{6} \times \sqrt{\frac{\sigma}{\rho g}} = 2.45 \times L_\sigma = 6.54 \times 10^{-3} \text{ m (or 6.54 mm)} , \quad (4)$$

where  $L_\sigma = \sqrt{\sigma/(\rho g)} = 2.67 \text{ mm}$  is regarded as the capillary scaling length (cf. Longuet-Higgins et al. 1991; Bari and Robinson 2013; Simmons et al. 2015). In other words, the bubble diameter in water is expected to be about the same as the contact line diameter at the orifice edge, when the orifice diameter  $D \sim 6.54 \text{ mm}$ . One of the cases presented by Oguz and Prosperetti (1993) with computed data as well as images of bubble shapes is that with  $D = 4 \text{ mm}$ , which is not too far from that given in (4) and could serve as a reference for comparison.

#### 3.1.1 Case of $D = 4 \text{ mm}$

For orifice diameter  $D = 4 \text{ mm}$ , the reference values of  $V_F$  and  $d_F$  are  $89.67 \text{ } \mu\text{L}$  (or  $\text{mm}^3$ ) and  $5.55 \text{ mm}$  with  $Q_{crit} = 3768.77 \text{ } \mu\text{L/s}$  (assuming  $d_c = D$ ) Figure 2 shows the computed results visualized with ParaView for bubble formation dynamics at various gas flow rates. As indicated by the spacing between the sequential bubbles, the bubble volume is increasing with the gas flow

rate because the spacing does not decrease inversely proportional to the gas flow rate. For low gas flow rates  $Q < Q_{crit}$ , the detached bubbles rise following one another in a so-called period-1 regime with the bubble volume gradually increasing with  $Q$  (as shown in table 1). When  $Q \sim Q_{crit}$  (i.e., at  $U = 300$  mm/s), the spacing between bubbles become so close that coalescence of two neighboring bubbles occurs and resulting in pairing bubbles in the period-2 regime (cf. Buwa et al. 2007). If the gas flow rate were further increased, it would eventually lead to chaos via period doubling (cf. Tufaile and Sartorelli 2000).

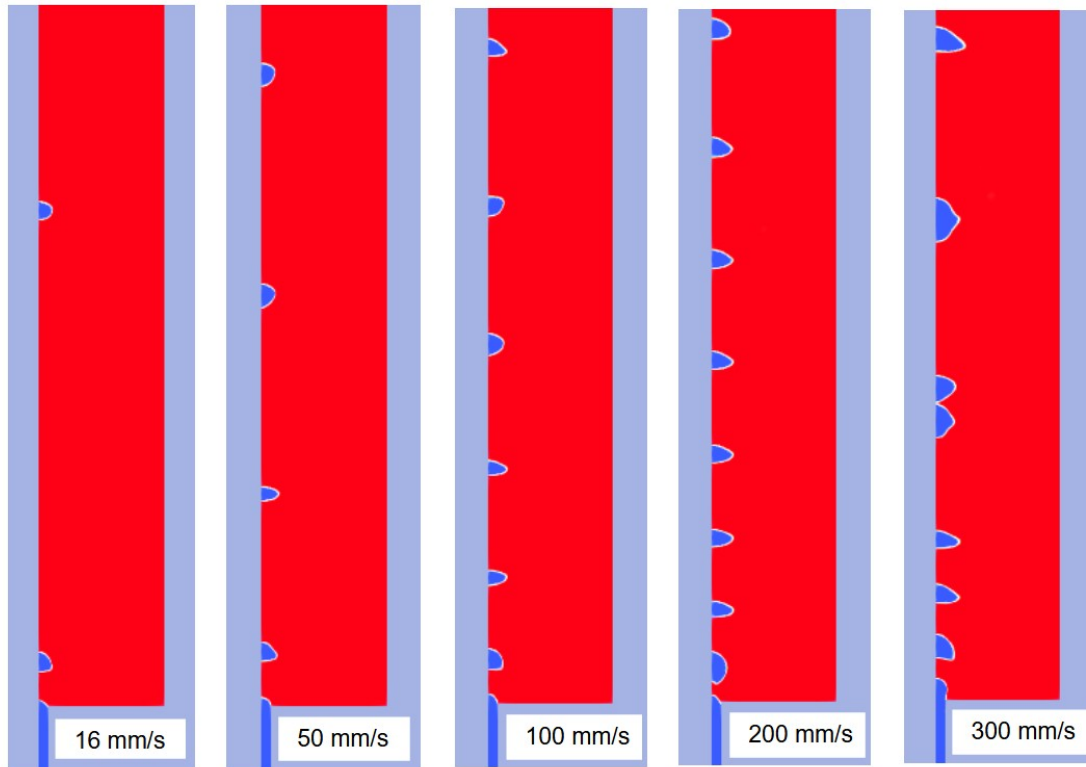


Figure 2. Formation of air bubbles in water from an orifice of diameter  $D = 4$  mm at various air flow velocity (i.e.  $U = 0.016, 0.05, 0.1, 0.2, 0.3$  m/s corresponding to flow rate  $Q = 201, 628, 1257, 2513, 3770$   $\mu\text{L/s}$ ), simulated with the OpenFOAM<sup>®</sup> VOF solver interIsoFoam and visualized with the postprocessor ParaView.

To provide more quantitative information, computed data of bubble detachment period  $\Delta T$  from which the corresponding bubble volume  $V$  and diameter  $d$  are derived according to the gas flow rate  $Q$  (i.e.,  $V = \Delta T \times Q$  which matches the numerical integration result along the free surface of a detached bubble) are given in table 1, with a reference to the  $Q / Q_{crit}$  value for  $D = 4$  mm. In comparison with the results by Oguz and Prosperetti (1993) for  $Q = 0.008$  and  $0.016$

$\mu\text{L/s}$  as  $d = 5.188$  and  $5.277$  mm, the present results of  $d = 4.71$  and  $4.81$  mm are consistently smaller (by about 10%). Despite the numerical differences between those values and that of Oguz and Prosperetti (1993), we are in agreement on the general trend of bubble volume  $V$  and corresponding diameter  $d$  decreasing with reducing  $Q$ . Both of our values of  $V$  and  $d$  are less than the corresponding  $V_F (= 89.67 \mu\text{L})$  and  $d_F (= 5.55 \text{ mm})$  from (1) which are usually regarded as the minimum values of bubble volume and diameter at the limit of so-called static bubble formation (at  $Q \ll Q_{crit}$ ), which were explained theoretically as the inaccuracy of quasi-static treatment for the dynamic process of necking and pinch-off by Simmons et al. (2015) with a model of pinned contact line. That the Fritz volume  $V_F$  needs correction was recognized in an early publication of Harkins and Brown (1919). More experimental evidence for  $V < V_F$  mostly with  $Q / Q_{crit} < 0.1$  has also been shown in publications of Corchero et al. (2006), Bari and Robinson (2013), and Manoharan et al. (2021). According to the fitted power law of Bari and Robinson (2013) for measured bubble volume  $V_B$  in experiments

$$\frac{V_B}{V_F} = 0.6863 \left( \frac{D}{L_\sigma} \right)^{-0.116}, \quad (5)$$

the value of  $V_B$  would become  $\sim 54.49 \text{ mm}^3$  for  $D = 4 \text{ mm}$  (with the capillary length in (4)  $L_\sigma = 2.67 \text{ mm}$ ), in agreement with the value of  $V$  in table 1 for  $Q \ll Q_{crit}$ .

Table 1. Computational results of bubble detachment period  $\Delta T$ , corresponding bubble volume  $V$  and bubble diameter  $d$  with a reference to the value of  $Q / Q_{crit}$  for  $D = 4 \text{ mm}$  (at  $\theta_0 = 45^\circ$ )

$U$ (m/s)	$Q$ ( $\mu\text{L/s}$ )	$\Delta T$ (ms)	$V$ ( $\text{mm}^3$ )	$d$ (mm)	$Q / Q_{crit}$
0.008	100.5	545	54.79	4.71	0.0266
0.016	201.1	289	58.11	4.81	0.0533
0.05	628.3	113	71.00	5.14	0.167
0.1	1256.6	68	85.45	5.46	0.333
0.2	2513.3	50	125.66	6.21	0.667
0.3	3769.9	41	154.57	6.66	1.000

If the data in table 1 is plotted in terms of  $V$  versus  $x = Q / Q_{crit} (< 1)$ , a fitted line can be obtained as  $V(x) = 103.84 x + 52.71 \text{ mm}^3$  with  $R^2 > 0.997$ . Thus, the present results suggest a monotonic increase of  $V$  with  $Q$  and  $V(0) = 52.71 \text{ mm}^3$ , unlike what has been claimed by most other authors as the static regime wherein  $V$  becomes nearly constant for  $Q / Q_{crit} \ll 1$ . According to the data in table 1, the bubble size may become close to those of the Fritz value (1) in the  $Q / Q_{crit}$  interval between 0.1 and 0.5. The deviation of  $V$  from  $V(0)$  would be  $< 10\%$  for  $Q / Q_{crit} < 0.05$ .

Bubble free surface profiles are shown in figure 3 during bubble detachment process at  $U = 0.008, 0.016, 0.1$  m/s. A series of bubble surface profiles for  $U \sim 0.016$  m/s ( $Q \sim 200$   $\mu\text{L/s}$ ) were presented by Oguz and Prosperetti (1993), qualitatively comparable to the corresponding profiles in figure 3. However, obvious discrepancy exists between their free surface shapes and figure 4 during attached bubble growth at particular time points, especially for  $t < -10$  ms. A closer examination reveals an inconsistency in their reported numerical free surface shapes which were apparently intended for comparison with the experimental images by Longuet-Higgins et al. (1991) for about one bubble per second, likely with  $Q < 60$   $\mu\text{L/s}$  rather than  $\Delta T \sim 300$  ms with  $Q \sim 200$   $\mu\text{L/s}$ . Figure 4 shows that a well-developed neck appears at free surface typically when  $t > -10$  ms, thereafter the time that takes for neck pinch-off would be almost independent of air flow rate but controlled by the capillary timescale (cf. Oguz and Prosperetti 1993),

$$t_\sigma = \sqrt{\frac{\rho D^3}{8\sigma}}, \quad (6)$$

which becomes 10.69 ms for  $D = 4$  mm (with  $\rho = 1000$   $\text{kg m}^3$  and  $\sigma = 0.07$   $\text{kg s}^{-2}$ ).

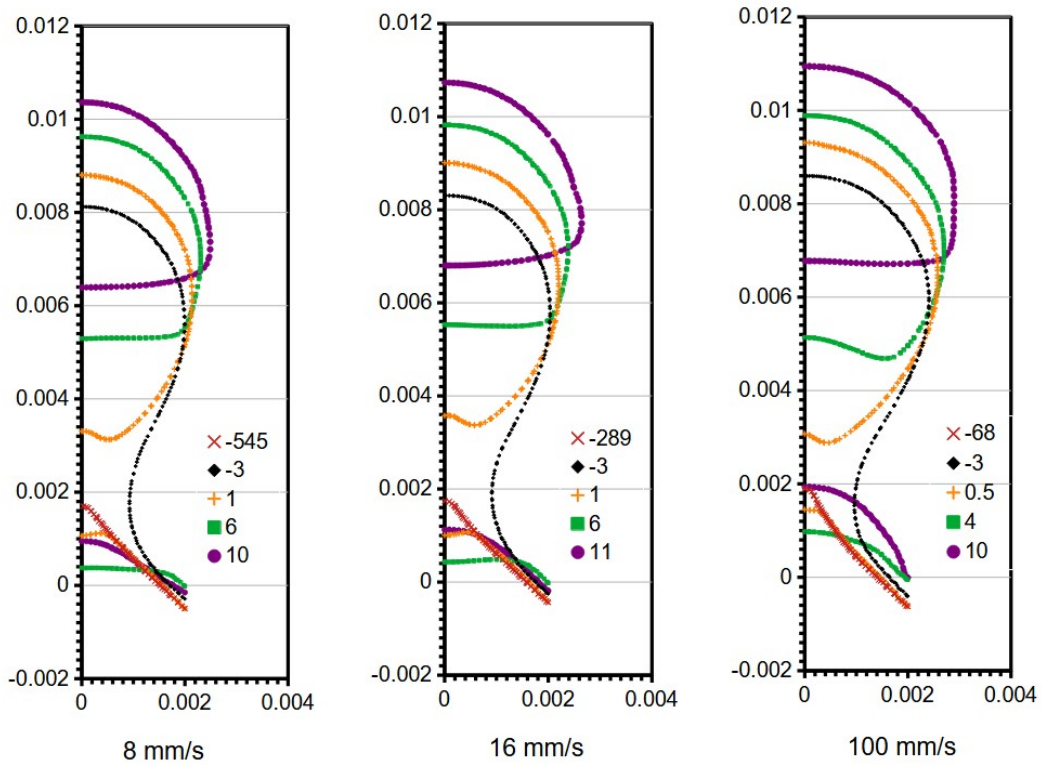


Figure 3. Free surface shapes during air bubble formation from an orifice of diameter  $D = 4$  mm in water at  $U = 0.008, 0.016, 0.1$  m/s corresponding to  $Q = 100.5, 201, 1257$   $\mu\text{L/s}$ .



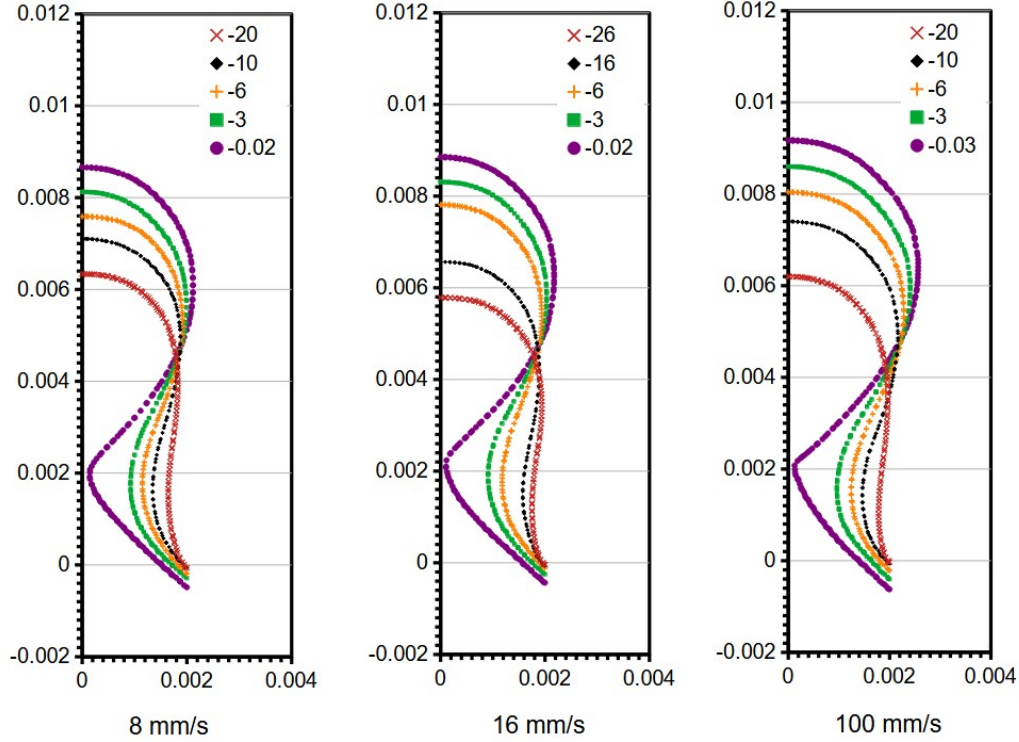


Figure 4. As figure 3 but only for during bubble growth toward necking pinch-off.

With the default setting of contact angle  $\theta_0 = 45^\circ$  (with  $\theta_A = 60^\circ$  and  $\theta_R = 30^\circ$ ), figures 3 and 4 also reveal the fact that the three-phase contact line could move along the vertical inner wall of the inlet tube, which apparently has not been mentioned in the published literature. The dynamic contact line seems to reach the deepest location ( $r = 2$  mm,  $z = -0.43$  mm for  $U = 0.016$  m/s) into the inner tube wall as the bubble detachment occurs, while outside the time interval of  $-t_\sigma < t < t_\sigma$  (where  $t_\sigma \sim 11$  ms) the contact line appears to stay pinned at the orifice edge ( $r = 2$  mm,  $z = 0$ ).

In view of the fact that Oguz and Prosperetti (1993) used a ‘90°-rule’ for contact angle, a case of  $\theta_0 = 90^\circ$  is computed for  $U = 0.016$  m/s ( $Q = 201$   $\mu\text{L/s}$ ). The results show  $\Delta T = 292$  ms with  $V = 58.71$  mm<sup>3</sup> and  $d = 4.82$  mm, which are practically no difference from the corresponding values in table 1. However, with  $\theta_0 = 90^\circ$  the contact line would be pinned at the orifice edge all the time (referred to as ‘mode A’ bubble formation in Gerlach et al. 2005), in contrast to the case of  $\theta_0 = 45^\circ$  in figures 3 and 4. The bubble surface profiles shown by Oguz and Prosperetti (1993) for this case indeed seem to have pinned contact line at the thin-wall

needle edge. According to the present results, the detached bubble volume at a given gas flow rate does not seem to vary much when the liquid is wetting the orifice wall with the contact angle less than that for contact line pinning at the orifice edge, because the contact diameter  $d_c$  remains the same as  $D$ .

If the contact angle is increased to  $\theta_0 = 120^\circ$  with  $U = 0.016$  m/s ( $Q / Q_{crit} = 0.0533$ ), we would now obtain  $\Delta T = 483$  ms with  $V = 97.11$  mm<sup>3</sup> and  $d = 5.70$  mm, while the contact line could reach as far as  $r \sim 4$  mm along the horizontal surface of  $z = 0$  during the time outside the interval  $(-t_\sigma, t_\sigma)$ . For  $\theta_0 = 105^\circ$ , we then obtain  $\Delta T = 347$  ms with  $V = 69.77$  mm<sup>3</sup> and  $d = 5.11$  mm, also with contact line moving on the horizontal surface. Actually, the contact line could move on the horizontal surface when  $\theta_0 > 95^\circ$  (for  $\theta_0 = 95^\circ$ , the contact line appears to be pinned at orifice edge and the value of  $\Delta T$  is within a few percent of that for  $\theta_0 = 45^\circ, 90^\circ$ ). The situation when the contact line moves on the horizontal surface during bubble formation is referred to as ‘mode B’ in Gerlach et al. (2005). In mode B the bubble volume was shown to increase with the contact angle almost exponentially from  $\theta_0 \sim 50^\circ$  to  $110^\circ$  (Gerlach et al. 2007), because the time-dependent contact diameter  $d_c$  is always greater than the orifice diameter  $D$ .

Under a given condition, there exists a critical contact angle  $\theta_c$  (e.g.,  $\sim 95^\circ$  for  $D = 4$  mm at  $U = 0.016$  m/s) dividing the Mode A and B regimes, namely below  $\theta_c$  the contact line could move along the vertical inner wall of inlet channel whereas above  $\theta_c$  the contact line is moving on the horizontal surface. The motion of contact line along the vertical inner wall has little effect on detached bubble size; but the bubble size can be very sensitive to the contact line motion on the horizontal surface due to transient variation of the contact diameter. The fact that below a critical contact angle  $\theta_c$  the detached bubble size appears independent of the contact angle was also reported by Manoharan et al. (2021).

### 3.1.2 Case of $D = 2$ mm

For  $D = 2$  mm, the reference values of  $V_F$  and  $d_F$  are  $44.83$   $\mu\text{L}$  (or mm<sup>3</sup>) and  $4.41$  mm with  $Q_{crit} = 2115.15$   $\mu\text{L/s}$  and  $t_\sigma = 3.78$  ms. To compare with a result of  $d = 4.40$  mm for  $Q \sim 391$   $\mu\text{L/s}$  by Oguz and Prosperetti (1993), a case of  $\theta_0 = 90^\circ$  is computed for  $U = 0.125$  m/s ( $Q = 392.70$   $\mu\text{L/s}$ ) which yields  $\Delta T = 147$  ms with  $V = 57.73$  mm<sup>3</sup> and  $d = 4.80$  mm. For  $\theta_0 = 80^\circ$ ,  $\Delta T = 101$  ms with  $V = 39.66$  mm<sup>3</sup> and  $d = 4.23$  mm. But the contact line would move on the horizontal surface for  $\theta_0 > 60^\circ$  (at  $\theta_0 = \theta_c \sim 60^\circ$  the contact line appears pinned at the orifice edge with computed  $\Delta T = 80$  ms). The value of  $\theta_{crit}$  seems to decrease with reducing orifice size. As a reference, the value of  $V_B$  from (5) would become  $\sim 29.53$  mm<sup>3</sup> for  $D = 2$  mm at low gas flow rates.

Table 2 presents the computed results for  $Q \sim 393$  and  $1668$   $\mu\text{L/s}$  each at  $\theta_0 = 45^\circ$  and  $75^\circ$ , respectively. The former is intended to compare with a case reported by Oguz and Prosperetti (1993). while the latter to compare with some results of Gerlach et al. (2007) who reported  $\Delta T = 42, 54, 126$  ms for  $\theta_0 = 0^\circ, 70^\circ, 110^\circ$ , respectively at  $Q = 1667$   $\mu\text{L/s}$  (100 mL/min) with their numerical simulations using a static contact angle model (i.e., for  $\theta_A = \theta_R = \theta_0$ ).

Clearly, the present results appear to consistently show smaller bubble volume than those reported by both Oguz and Prosperetti (1993) as well as Gerlach et al. (2007). Although the governing equations for the bubble formation problem are mostly the same, the treatments of dynamic behavior of the contact line are noticeably different between the present model and those previous authors. Before resolving the exact causes (which can be extremely difficult due to inaccessible source codes), the differences beyond normally acceptable numerical tolerance may be attributed to the differences in mathematical representation of dynamic contact line, for now. Nonetheless, the present results are in qualitative agreement with the previous publications with the same trends for variations of wetting angle and gas flow rate.

Table 2. As table 1 but for  $D = 2$  mm with  $V_F = 44.83$   $\mu\text{L}$ ,  $d_F = 4.41$  mm,  $Q_{crit} = 2115.15$   $\mu\text{L/s}$ .

$U$ (m/s)	$Q$ ( $\mu\text{L/s}$ )	$\theta_0$ (deg)	$\Delta T$ (ms)	$V$ ( $\text{mm}^3$ )	$d$ (mm)	$Q / Q_{crit}$
0.125	392.70	45	80	31.42	3.91	0.186
		75	93	36.52	4.12	
0.531	1668.18	45	36	60.05	4.86	0.789
		75	47	78.40	5.31	

To provide a reference for the “static regime” at low gas flow rate situation (where the bubble size has little variations), a case of  $U = 0.05$  m/s ( $Q / Q_{crit} = 0.0743$ ) is computed yielding bubble diameters  $d = 3.81$  mm corresponding to a volume  $V = 28.90$   $\text{mm}^3$  for  $\Delta T = 184$  ms with  $\theta_0 = 45^\circ$  (which is practically the same as that up to  $\theta_0 = 75^\circ$ ). Apparently, the critical contact angle  $\theta_c \sim 75^\circ$  (for the contact line pinned at the orifice edge) could increase somewhat with reducing the gas flow rate. But with  $\theta_0 = 90^\circ$  significant contact line motion on horizontal surface occurs, as a consequence the computed  $d = 4.59$  mm,  $V = 50.74$   $\text{mm}^3$  with  $\Delta T = 323$  ms. Actually the contact line motion on horizontal surface becomes obvious at  $\theta_0 = 80^\circ$  with  $\Delta T = 219$  ms,  $V = 34.40$   $\text{mm}^3$  and  $d = 4.04$  mm. Apparently, the present results for partially wetting liquids with  $\theta_0 < \theta_c$  are in good agreement with the value of  $V_B \sim 29.53$   $\text{mm}^3$  from (5) for  $D = 2$  mm.

Further comparison with some computed bubble surface profiles in Fig. 3 of Gerlach et al. (2007) for  $\theta_0 = 0^\circ, 70^\circ$ , and  $110^\circ$  at  $Q = 1667$   $\mu\text{L/s}$  and  $t = 0, \Delta T/3, 2 \Delta T/3$  is provided in figure 5 as present computational results for  $\theta_0 = 45^\circ, 75^\circ$ , and  $105^\circ$  exhibiting similar contact line motion on the horizontal surface (which could occur for  $\theta_0 > 60^\circ$  per present computations). The bubble surface profiles in figure 5 look generally comparable to those of Gerlach et al. (2007).

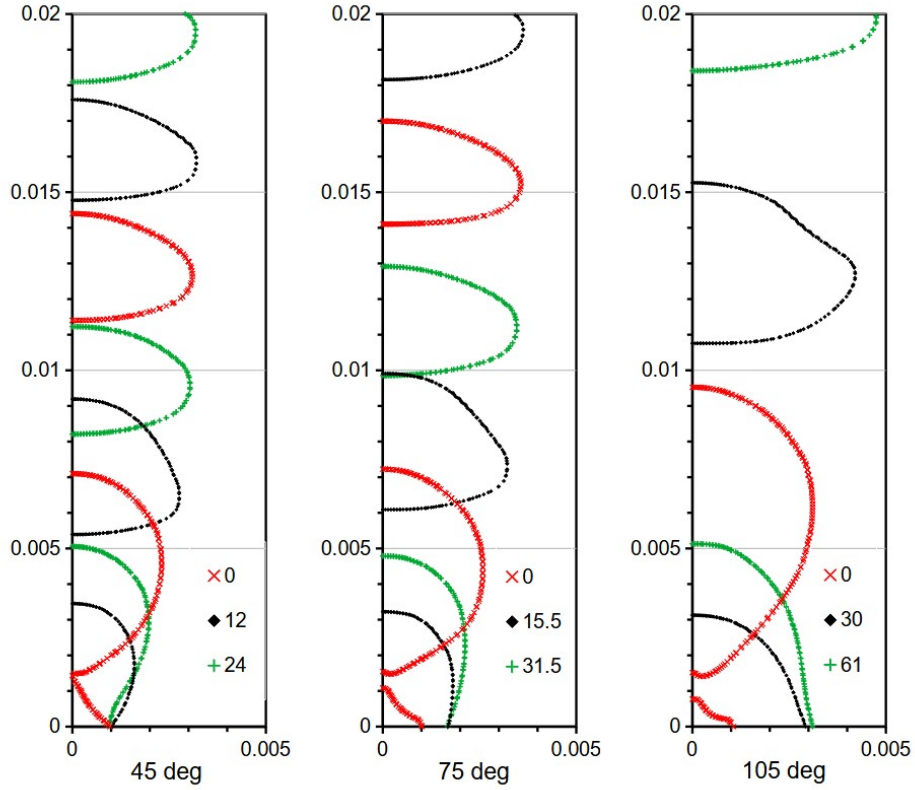


Figure 5. As figure 3 but for  $D = 2$  mm at  $U = 0.531$  m/s corresponding to flow rate  $Q = 1668$   $\mu\text{L/s}$  for  $\theta_0 = 45^\circ, 75^\circ, 105^\circ$  (with  $\theta_l = \theta_0 + 15^\circ$  and  $\theta_r = \theta_0 - 15^\circ$ ) and  $\Delta T = 36, 47, 91$  ms.

For the record, a fitted line can be obtained as  $V(x) = 44.24x + 24.49$   $\text{mm}^3$  with  $R^2 > 0.997$  for  $\theta_0 = 45^\circ$  and  $D = 2$  mm with data at  $Q / Q_{crit}$  from 0.037 up to 1.04. Unlike that seen in figure 2 for  $D = 4$  mm at  $Q / Q_{crit} = 1$  with pairing bubbles, here the detached bubbles remain period-1 when  $Q / Q_{crit} = 1.04$  for  $D = 2$  mm (with pairing bubbles observed at  $Q / Q_{crit} = 1.485$  when a slight movement of the contact line can be noticed on the horizontal surface).

### 3.1.3 Case of $D = 1.5$ mm

In a study of the wetting effects on bubble formation, Manoharan et al. (2021) presented experimental results for a list of averaged bubble diameters detached from  $D = 1.5$  mm with different contact angles with respect to water, in the static regime (for  $Q < 150$   $\mu\text{L/s}$  or  $< 9$  mL/min):  $d = 2.75, 2.69, 2.98, 3.78, 3.98, 4.27$  mm with  $\theta_0 = 43^\circ, 52^\circ, 62^\circ, 105^\circ, 120^\circ, 128^\circ$  (in their Table 2). For  $D = 1.5$  mm, we would have  $V_F = 33.63$   $\mu\text{L}$  and  $d_F = 4.00$  mm with  $Q_{crit} = 1664.28$   $\mu\text{L/s}$  and  $t_\sigma = 2.45$  ms. Yet the value of  $d = 3.52$  mm corresponding to  $V_B = 22.90$   $\text{mm}^3$

from (5) for  $D = 1.5$  mm, which seems in reasonable agreement with the results shown in table 3 for  $\theta_0 < 65^\circ$  (i.e., in this case the value of  $\theta_c \sim 65^\circ$ ). Noteworthy here is that at  $\theta_0 = 70^\circ$  even with noticeable contact line motion on the horizontal surface the computed bubble size does not seem to change from that for  $\theta_0 < 65^\circ$  (for  $D = 1.5$  mm with  $Q / Q_{crit} = 0.053$  corresponding to  $U = 0.05$  m/s). In this case, the contact line motion on the horizontal surface occurs only when  $\sim 15$  ms away from the time of meniscus pinch-off, much longer than  $t_\sigma = 2.45$  ms.

Table 3. As table 1 but for  $D = 1.5$  mm with  $V_F = 33.63$   $\mu\text{L}$ ,  $d_F = 4.00$  mm,  $Q_{crit} = 1664.28$   $\mu\text{L/s}$ .

$U$ (m/s)	$Q$ ( $\mu\text{L/s}$ )	$\theta_0$ (deg)	$\Delta T$ (ms)	$V$ ( $\text{mm}^3$ )	$d$ (mm)	$Q / Q_{crit}$
0.05	88.36	45	218	19.26	3.32	0.053
		60	214	18.91	3.31	
		75	283	25.01	3.63	
		90	540	47.71	4.50	
		105	888	78.46	5.31	
		120	884	78.11	5.30	

It is interesting to note that the bubble sizes in table 3 are consistently greater than those corresponding ones shown by Manoharan et al. (2021), unlike many other comparisons with previously published data. However, the present results for  $\theta_0 < 75^\circ$  are in quite good agreement with the value of  $V_B$  according to (5) based on the experiments of Bari and Robinson (2013) which were seemingly done with  $\theta_0 < 75^\circ$ .

### 3.1.4 Case of $D = 1$ mm

Reducing orifice size to  $D = 1$  mm would have  $V_F = 22.42$   $\mu\text{L}$  and  $d_F = 3.50$  mm with  $Q_{crit} = 1187.09$   $\mu\text{L/s}$  and  $t_\sigma = 1.34$  ms, while  $V_B = 16.00$   $\mu\text{L}$  (corresponding to  $d = 3.13$  mm) from (5) for  $Q \ll Q_{crit}$  and seemingly  $\theta_0 < 70^\circ$ . Table 4 shows the computed results for  $D = 1$  mm at  $Q / Q_{crit} = 0.033$  and various  $\theta_0$  with  $\theta_c < 60^\circ$  (at  $\theta_0 = 60^\circ$  the contact line motion on horizontal surface is noticeable although the detached bubble volume does not seem to increase). Noteworthy here is that even at  $\theta_0 = 65^\circ$  with substantial contact line movements on horizontal surface, the detached bubble volume still remains comparable to that at  $\theta_0 = 45^\circ$ . It is up to  $\theta_0 = 70^\circ$  the detached bubble volume becomes about the same as  $V_B$ .

Corchero et al. (2006) presented some experimental results of bubble formation in water for  $D = 1$  mm at  $Q = 48.4$   $\mu\text{L/s}$  ( $U \sim 0.0616$  m/s) with  $\theta_0 = 68^\circ$  yielding bubbles of  $V \sim 22.4$   $\text{mm}^3$

and  $d \sim 3.5$  mm, among others. This is quite comparable to  $V_F$  and  $d_F$  which would happen at  $\theta_0 \sim 75^\circ$  according to present results shown in table 4. Imperfect quantitative comparison between the computational model and experiment may not be surprising in view of the intrinsic limitations of macroscopic continuum models for the dynamic contact line (cf. Blake and Ruschak 1997; Chen et al. 2009) as well as difficulties in experimentally measuring the moving contact line behavior. Now it is clear that the preferred comparison cases would be those with  $\theta_0 < \theta_c$  where the detached bubble sizes are insensitive to the actual  $\theta_0$  value, and also practically desirable for minimizing the bubble size. However, it should be noted that the value of  $\theta_c$  for contact line pinning is likely to depend on dynamic contact line formulation in computational models and surface properties of the orifice materials in experiments.

Table 4. As table 1 but for  $D = 1$  mm with  $V_F = 22.42$   $\mu\text{L}$ ,  $d_F = 3.50$  mm,  $Q_{crit} = 1187.09$   $\mu\text{L/s}$ .

$U$ (m/s)	$Q$ ( $\mu\text{L/s}$ )	$\theta_0$ (deg)	$\Delta T$ (ms)	$V$ ( $\text{mm}^3$ )	$d$ (mm)	$Q / Q_{crit}$
		45	274	10.76	2.74	
0.05	39.27	65	282	11.07	2.77	0.033
		70	419	16.45	3.16	
		75	586	23.01	3.53	

To examine the effect of gas flow rate  $Q$  for  $\theta_0 < \theta_c$  cases at  $\theta_0 = 45^\circ$  with  $Q = 392.7$   $\mu\text{L/s}$  ( $U = 0.5$  m/s,  $Q / Q_{crit} = 0.331$ ),  $Q = 1178.1$   $\mu\text{L/s}$  ( $U = 1.5$  m/s,  $Q / Q_{crit} = 0.992$ ), and  $Q = 1570.8$   $\mu\text{L/s}$  ( $U = 2$  m/s,  $Q / Q_{crit} = 1.323$ ) are also computed here. As already being observed, with increasing  $Q / Q_{crit}$  to  $> 0.992$  the value of  $\theta_c$  would be reduced to  $< 45^\circ$ , because now at  $\theta_0 = 45^\circ$  the contact line motion is noticeable on the horizontal surface.

Again, the computed data at  $Q / Q_{crit} = 0.033, 0.331, 0.992, 1.323$  for  $\theta_0 = 45^\circ$  can be fitted into a line of  $V$  versus  $x = Q / Q_{crit}$  as  $V(x) = 21.45 x + 9.179$   $\text{mm}^3$  with  $R^2 > 0.995$ . The phenomenon of bubble pairing for an orifice of  $D = 1$  mm with  $\theta_0 = 45^\circ$  does not seem to occur until  $Q / Q_{crit} > 2$ , and definitely occurs when  $U = 3.5$  m/s corresponding to  $Q / Q_{crit} = 2.32$  with  $\Delta T = 23.6$  ms,  $V = 64.87$   $\text{mm}^3$  and  $d = 4.99$  mm (which is above but not too far from the fitted linear formula  $V(2.32) = 58.85$   $\text{mm}^3$ ). It should be noted that the value of  $V$  here is obtained from neck pinch-off period  $\Delta T$  for individual bubbles before pairing coalescence. Apparently, the value of  $Q / Q_{crit}$  for pairing bubbles increases with reducing the orifice size. The fitted linear formula based on values of  $V$  versus  $x$  up to  $Q / Q_{crit} \sim 1$  seems to be also valid for larger  $Q / Q_{crit}$  values. At  $Q / Q_{crit} = 2.32$  when bubble pairing occurs, the contact line is noticeably moving on the horizontal orifice surface even with  $\theta_0 = 45^\circ$ , again indicating that the value of  $\theta_c$  would decrease with increasing  $Q$ .

Mirsandi et al. (2020) showed experimental as well as computational results for  $D = 1$  mm around  $Q = 21.8$   $\mu\text{L/min}$  (i.e., 363  $\mu\text{L/s}$  and  $U \sim 0.462$  m/s) with  $\theta_0 \sim 105^\circ$  and  $\Delta T \sim 351$

ms, apparently corresponding to bubbles of  $V \sim 127 \text{ mm}^3$  and  $d \sim 6.2 \text{ mm}$ . For a comparison, a case of  $U = 0.462 \text{ m/s}$  at  $\theta_0 \sim 105^\circ$  (with  $\theta_A = 120^\circ$  and  $\theta_R = 90^\circ$ ) is computed here yielding bubbles of  $V = 87.08 \text{ mm}^3$  and  $d = 5.50 \text{ mm}$ , significantly larger than that with  $\theta_0 = 45^\circ$  (i.e., having  $V(0.306) \sim 15.5 \text{ mm}^3$ ) but not quite as large as that of Mirsandi et al. If the value of  $D$  were increased to 2 mm and 4 mm with all others kept the same, the resulting  $d$  would respectively become 5.63 and 5.57 mm, not really much different from  $d = 5.50 \text{ mm}$  with  $D = 1 \text{ mm}$ . Then, for non-wetting liquids with respect to the orifice wall, the bubble size may not decrease with reducing the orifice size at a given gas flow rate.

### 3.2 Air bubbles in an aqueous-glycerol solution

For air bubbles forming from an orifice of  $D = 1.7 \text{ mm}$  in an aqueous-glycerol solution with  $\rho = 1223.8 \text{ kg m}^{-3}$ ,  $\sigma = 0.066 \text{ kg s}^{-2}$ , and  $\mu = 0.126 \text{ kg m}^{-1} \text{ s}^{-1}$  (Helsby and Tuson 1955; Ohta et al. 2011), the values of  $V_F$  and  $d_F$  become  $29.36 \text{ }\mu\text{L}$  and  $3.83 \text{ mm}$ . According to (3) the Ohnesorge number in this case would take a value of  $Oh = 0.2895$ , much larger than  $2.313 \times 10^{-3}$  for the air-water system. This is an exemplifying case for the effect of increasing viscosity by two orders of magnitude.

Table 5. As table 1 but for  $D = 1.7 \text{ mm}$ ,  $\rho = 1223.8 \text{ kg m}^{-3}$ ,  $\sigma = 0.066 \text{ kg s}^{-2}$ , and  $\mu = 0.126 \text{ kg m}^{-1} \text{ s}^{-1}$  with  $V_F = 29.36 \text{ }\mu\text{L}$ ,  $d_F = 3.83 \text{ mm}$ ,  $Q_{crit} = 1486.40 \text{ }\mu\text{L/s}$ .

$U \text{ (m/s)}$	$Q \text{ (}\mu\text{L/s)}$	$\theta_0 \text{ (deg)}$	$\Delta T \text{ (ms)}$	$V \text{ (mm}^3\text{)}$	$d \text{ (mm)}$	$Q / Q_{crit}$
0.088	199.74	45	140.5	28.06	3.77	0.134
		75	171	34.16	4.03	
0.441	1000.98	45	60.5	60.56	4.87	0.673
		75	72	72.07	5.16	
0.881	1999.69	45	48.2	96.39	5.69	1.345
		75	56.0	111.98	5.98	

Table 5 shows the present model results for  $U = 0.088, 0.441, 0.881 \text{ m/s}$  at  $\theta_0 = 45^\circ$  and  $75^\circ$ , for comparing with a set of computational results reported by Ohta et al. (2011), i.e.,  $d = 4.22, 4.89, 5.49 \text{ mm}$ , and corresponding experimental results of Helsby and Tuson (1955) as  $d = 4.06, 4.99, 5.72 \text{ mm}$ . In view of the fact that both Helsby and Tuson (1955) and Ohta et al. (2011) were considering bubble detaching from a thin-wall needle rather than an orifice on a plane surface, their results should correspond to the present cases of  $\theta_0 = 45^\circ$  with contact diameter remaining constant. But the cases of  $\theta_0 = 75^\circ$  are also computed here for references. Indeed, the present computations for  $\theta_0 = 45^\circ$  yield results in reasonable agreement with Helsby and Tuson

(1955) and Ohta et al. (2011), although at  $U = 0.088$  m/s the case of  $\theta_0 = 75^\circ$  seems to offer even better agreement. As expected from the discussion in subsection 3.1, the present values of  $V = 28.06$  mm<sup>3</sup> and  $d = 3.77$  mm at  $Q / Q_{crit} = 0.134$  are very close to  $V_F = 29.36$   $\mu$ L and  $d_F = 3.83$  mm.

Another observation from the computed results with  $Oh = 0.2895$  indicates that in a liquid of higher viscosity the bubbles exhibit little surface deformations from the spherical shape, as expected from viscous suppression of surface-tension driven oscillations. Here the computed bubble rising velocity is in the range of 0.1 to 0.2 m/s, comparable to those reported by Ohta et al. (2011). Thus, with  $\rho = 1223.8$  kg m<sup>-3</sup>,  $\sigma = 0.066$  kg s<sup>-2</sup>, and  $\mu = 0.126$  kg m<sup>-1</sup> s<sup>-1</sup> for a bubble of  $D = 4$  mm and rising velocity of 0.2 m/s, the estimated rising bubble Reynolds number would be  $Re \sim 9.7$  and Weber number  $We \sim 3.7$  which would not cause substantial steady-state bubble surface deformation (cf. Feng 2007), either.

### 3.3 Air bubbles in a liquid of lower surface tension

So far the computed cases are mostly relevant to air bubbles in aqueous liquids with surface tension around  $\sigma \sim 0.07$  kg s<sup>-2</sup>, because most available experimental data are with the air-water systems for laboratory convenience. The case of reduced surface tension computed here for  $D = 1$  mm and  $\theta_0 = 45^\circ$  at  $U = 0.05$  m/s is with  $\sigma = 0.035$  kg s<sup>-2</sup> (as representative to many non-aqueous solvents) and everything else remains the same as that for the air-water systems in subsection 3.1.4, as a purely computational benchmark study against the corresponding case for  $\sigma = 0.07$  kg s<sup>-2</sup> with  $\Delta T = 274$  ms and  $V = 10.76$  mm<sup>3</sup> as in table 4. The resulting  $\Delta T$  becomes 152.5 ms with  $V = 5.99$  mm<sup>3</sup> which is about 10% greater than  $0.5 \times 10.76 = 5.38$  mm<sup>3</sup> as estimated by (1) for the quasi-static situation. Again, the Fritz formulas in (1), based on a force balance between surface tension and buoyancy, may only be useful for rough estimates rather than accurate predictions in specific applications, because other effects (cf. Mohseni et al. 2020) would be more influential especially with reduced surface tension.

## 4 Summary

The OpenFOAM<sup>®</sup> VOF computational model presented here seems to yield numerical results in general qualitative agreement with most of those reported by previous authors, which in some sense verifies the model validity. For example, the present results show that the detached bubble size tends to increase with the gas flow rate, orifice size, surface tension, liquid contact angle, etc. There exists a critical gas flow rate above which detached bubbles will combine via coalescence and exhibit the bubble pairing phenomenon. The detached bubble size seems insensitive to the liquid contact angle when it is smaller than a critical value (referred to as Mode A), but can increase substantially at larger contact angles which result in the contact line movement on the horizontal orifice surface (Mode B per Gerlach et al. 2005). To avoid deeply involving into complexities with the Mode B bubble formation process, the present work mainly focuses on analyzing the Mode A cases with a few Mode B cases computed for brief demonstrative purposes. Operating with the Mode A is desirable for the convenience of control



and minimizing the bubble size, and can be accomplished by using orifice materials that allow adequate liquid wetting.

On the other hand, the present computational study also reveals certain details apparently not yet recognized in relevant publications. Majority publications in the literature tend to confirm the claim that the detached bubble volume would become about the same as the Fritz value  $V_F$  in (1) irrespective of gas flow rate when  $Q / Q_{crit} < 1$ , whereas the present study shows linear relationship between  $V$  and  $Q$  with noticeable slope that increases with orifice size (cf. Table 6 based on results for  $\theta_0 = 45^\circ$  when the liquid ‘wets’ the orifice walls). It becomes clear that the slope of the fitted line increases with the orifice size. Another clear indication here is that the detached bubble volume for  $Q / Q_{crit} \ll 1$  tends to be considerably smaller than  $V_F$  as seemingly in agreement with the experiments of Bari and Robinson (2013). If further independently confirms, this finding could be a good news because smaller bubbles with a given orifice size is often desirable for heat and mass transfer applications.

Table 6. Fitted values of  $a$  and  $b$  in linear relationship of  $V$  versus  $x = Q / Q_{crit}$  as  $V(x) = a x + b$  for  $D = 1, 2, 4$  mm with  $x$  up to 1 (or not too far above 1), based on results for  $\theta_0 = 45^\circ$  .

$D$ (mm)	$Q_{crit}$ ( $\mu\text{L/s}$ )	$a$ ( $\text{mm}^3$ )	$b$ ( $\text{mm}^3$ )	$V_F$ ( $\text{mm}^3$ )
1	1187.09	21.446	9.179	22.42
2	2115.15	44.239	24.493	44.83
4	3768.77	103.84	52.710	89.67

However, having smaller bubbles requires using relatively lower gas flow rates (e.g., with  $Q / Q_{crit} < 0.1$ ), which would compromise the bubble throughput per orifice as an important factor to consider in process development. Moreover, the present results also show that the critical contact angle  $\theta_c$  dividing Mode A and B bubble formation regimes shrinks with reducing the orifice size as well as increasing the gas flow rate. Such a fact would make the usage of reduced orifice size for generating smaller bubbles more challenging and practically difficult with constant gas flow for  $D < 1$  mm. This appears to be consistent with the experiments of Mohseni et al. (2020) with laser machined sub-millimeter orifices on stainless steel plates in water with measured  $\theta_0 \sim 75^\circ$ , bubbles detached from a  $D = 0.4$  mm orifice could have  $V \sim 21, 27, 32 \text{ mm}^3$  at  $Q = 167, 500, 833 \text{ }\mu\text{L/s}$  (with  $Q_{crit} \sim 553 \text{ }\mu\text{L/s}$ ), generally larger than that from a  $D = 1$  mm orifice (cf. table 4) as a consequence of much higher gas flow rate than  $Q = 39.27 \text{ }\mu\text{L/s}$ .

## Statements and Declarations

**Competing interests** The author has no competing interests to declare.

## References

- Bari S D, Robinson A J (2013) Experimental study of gas injected bubble growth from submerged orifices. *Experimental Thermal and Fluid Science* 44: 124-137
- Blake T D, Ruschak K J (1997) Wetting: Static and dynamic contact lines. In *Liquid Film Coating—Scientific Principles and Their Technological Implications*. Ed. S F Kistler, P M Schweizer. Chapman & Hall, pp 62-97
- Buwa V V, Gerlach D, Durst F, Schlucker E (2007) Numerical simulations of bubble formation on submerged orifices: period-1 and period-2 bubbling regimes. *Chem. Eng. Sci.* 62: 7119-7132
- Chen Y, Mertz R, Kulenovic R (2009) Numerical simulation of bubble formation on orifice plates with a moving contact line. *Int. J. Multiphase Flow* 35: 66-77
- Christodoulou KN, Scriven LE (1992) Discretization of free surface flows and other moving boundary problems. *J. Comput. Phys.* 99: 39-55
- Clift R, Grace J R, Weber M E (1978) *Bubbles, Drops, and Particles*. Academic Press Inc., New York
- Corchero G, Medina A, Higuera FJ (2006) Effect of wetting conditions and flow rate on bubble formation at orifices submerged in water. *Colloids and Surfaces A: Physicochem. Eng. Aspects* 290: 41-49
- Das A K, Das P K, Saha P (2011) Formation of bubbles at submerged orifices—experimental investigation and theoretical prediction. *Exp. Therm. Fluid Sci.* 35: 618-627
- Feng JQ (2007) A spherical-cap bubble moving at terminal velocity in a viscous liquid. *J. Fluid Mech.* 579: 347-371
- Feng JQ (2017) A computational study of high-speed microdroplet impact onto a smooth solid surface. *J. Appl. Fluid Mech.* 10(1): 243-256
- Fritz W (1935) Berechnung des maximale volume dampfblasen (Calculation of maximum volume vapor bubbles). *Phys. Z.* 36: 379-384
- Gaddis E S, Vogelpohl A (1986) Bubble formation in quiescent liquids under constant flow conditions. *Chem. Eng. Sci.* 41(1): 97-105
- Gamet L, Scala M, Roenby J, Scheufler H, Pierson J-L (2020) Validation of volume-of-fluid OpenFOAM® isoAdvector solvers using single bubble benchmarks. *Comput. Fluids* 213: 104722
- Gerlach D, Biswas G, Durst F, Kolobraric V (2005) Quasi-static bubble formation on submerged orifices. *Int. J. Heat Mass Transfer.* 48: 425-438

- Gerlach D, Alleborn N, Buwa V, Durst F (2007) Numerical simulation of periodic bubble formation at a submerged orifice with constant gas flow rate. *Chem. Eng. Sci.* 62: 2109-2125
- Harkins W D, Brown F E (1919) The determination of surface tension (free surface energy) and the weight of falling drops: The surface tension of water and benzene by the capillary height method. *Journal of the American Chemical Society* 41: 499-525
- Higuera FJ (2005) Injection and coalescence of bubbles in a very viscous liquid. *J. Fluid Mech.* 530: 369-378
- Hirt CW, Nichols BD (1981) Volume of fluid (VOF) method for the dynamics of free boundaries. *J. Comput. Phys.* 39(1): 201-225
- Jamialahmadi M, Zehtaban M R, Muller-Steinhagen H, Sarrafi A, Smith J M (2001) Study of bubble formation under constant flow conditions. *Chem. Eng. Res. Des.* 79: 523-532
- Kistler SF, Scriven LE (1983) Coating flows. In *Computational Analysis of Polymer Processing*, Ed. JRA Pearson, SM Richardson, Springer, pp 243-299
- Krishna R, Urseanu MI, van Baten JM, Ellenberger J (1999) Rise velocity of a swarm of large gas bubbles in liquids. *Chem. Eng. Sci.* 54(2): 171-183
- Kulkarni A A, Joshi J B (2005) Bubble formation and bubble rise velocity in gas-liquid systems: a review. *Ind. Eng. Chem. Res.* 44: 5873-5931
- Kumar R, Kuloor N R (1970) The formation of bubbles and drops. *Adv. Chem. Engng.* 8: 256-368
- Longuet-Higgins MS, Kerman BR, Lunde K (1991) The release of air bubbles from an underwater nozzle. *J. Fluid Mech.* 230: 365-390
- Matkovic M, Koncar B (2012) Bubble departure diameter prediction uncertainty. *Science and Technology of Nuclear Installations*
- Manoharan S, Manglik R M, Jog M A (2021) Wetting and capillarity effects on bubble formation from orifice plates submerged in pools of water. *Transactions of the ASME Journal of Heat Transfer* 143: 101602
- Mirsandi H, Smit W J, Kong G, Baltussen M W, Peters E A J F, Kuipers J A M (2020) Influence of wetting conditions on bubble formation from a submerged orifice. *Experiments in Fluids* 61: 83
- Mohseni E, Kalayathine J J, Reinecke S F, Hampel U (2020) Dynamics of bubble formation at micro-orifices under constant gas flow conditions. *Int J Multiphase Flow* 132: 103407
- Mulbah C, Kang C, Mao N, Zhang W, Shaikh A R, Teng S. (2022) A review of VOF methods for simulating bubble dynamics. *Progress in Nuclear Energy* 154: 104478

Nichita BA, Zun I, Thome JR (2010) A level set method coupled with a volume of fluid method for modeling of gas-liquid interface in bubbly flow. *J. Fluids Eng.* 132(8): 081302

Oguz H N, Prosperetti A (1993) Dynamics of bubble growth and detachment from a needle. *J. Fluid Mech.* 257: 111-145

Ohta M, Kikuchi D, Yoshida Y, Sussman M (2011) Robust numerical analysis of the dynamic bubble formation process in a viscous liquid. *Int. J. Multiphase Flow* 37: 1059-1071

Ponter A B, Surati A I (1997) Bubble emissions from submerged orifices—a critical review. *Chem. Eng. Technol.* 20(2): 85-89

Roenby J, Bredmose H, Jasak H (2016) A computational method for sharp interface advection. *Royal Society Open Science* 3: 160405

Sethian JA (1999) *Level Set Methods and Fast Marching Methods: Evolving Interfaces in Computational Geometry, Fluid Mechanics, Computer Vision, and Materials Science.* Cambridge University Press

Simmons J A, Sprittles J E, Shikhmursaev Y D (2015) The formation of a bubble from a submerged orifice. *Euro. J. Mech. B/Fluids* 53: 24-36

Sudeepta Vaishnavi GNV, Ramarajan J, Jayavel S (2023) Numerical studies of bubble formation dynamics in gas-liquid interaction using volume of fluid (VOF) method. *Thermal Sci. Eng. Prog.* 39(1): 101718

Sussman M, Fatemi E, Smereka P, Osher S (1998) An improved level set method for incompressible two-phase flows. *Comput. Fluids* 27(5-6): 663-680

Sussman M, Puckett EG (2000) A coupled level set and volume-of-fluid method for computing 3D and axisymmetric incompressible two-phase flows. *J. Comput. Phys.* 162: 301-337

Tufaile A, Sartorelli J C (2000) Chaotic behavior in bubble formation dynamics. *Physica A: Statistical Mechanics and Its Applications* 275(3-4): 336-346

van Krevelen D, Hoftijzer P (1950) Studies of gas-bubble formation: calculation of interfacial area in bubble contractors. *Chem. Eng. Prog.* 46: 29-35

Wong H, Rumshitzki D, Maldaralli C (1998) Theory and experiment on the low-Reynolds number expansion and contraction of a bubble pinned at a submerged tube tip. *J. Fluid Mech.* 356: 93-124